Acta Crystallographica Section B
Structural Science
ISSN 0108-7681

Structural disorder of a new zeolite-like lithosilicate, $K_{2.6}Li_{5.4}[Li_4Si_{16}O_{38}]\cdot 4.3H_2O$

So-Hyun Park,[a]* Hans Boysen[a] and John B. Parise[b]

[a]Sektion Kristallographie, Department für Geo- und Umweltwissenschaften, Ludwig-Maximilians Universität München, 80333 München, Germany, and [b]Department of Geosciences, Department of Chemistry, State University of New York at Stony Brook, NY 11790-2100, USA

Correspondence e-mail: sohyun.park@physik.uni-muenchen.de

Received 15 September 2005
Accepted 22 November 2005

The framework structure of the synthetic microporous lithosilicate RUB-30 ($K_{2.6}Li_{5.4}[Li_4Si_{16}O_{38}]\cdot 4.3H_2O$) is similar to that of the fibrous zeolites such as natrolite, edingtonite and thomsonite, since all their frameworks include the same secondary structural building unit, the so-called 4–1 T_5O_{10} cluster of tetrahedra. Unique to the structure of RUB-30, each 4–1 unit consists of a $LiSi_4O_{10}$ moiety within which the single $[LiO_4]$ tetrahedron is strictly segregated from the other four $[SiO_4]$ tetrahedra. The connection of neighboring 4–1 units through edge-sharing $[LiO_4]$ tetrahedra results in a new framework topology. The present work reports an 'average' structure of RUB-30 solved by synchrotron X-ray single-crystal diffraction data collected at a second-generation source. A superstructure with $a \times 2b \times c$ (relative to the subcell quoted above) could be seen in X-ray diffraction data collected with better resolution and higher brightness at a third generation source. Diffuse streaks along k with l = odd and unusual superstructure hkl reflections, with k = odd and l = odd only, indicate a more complicated real structure of the material. To explain this observation we propose two different structure types which are statistically, but coherently, intergrown in RUB-30.

1. Introduction

Aside from the multifunctional uses as heterogeneous catalysts, ion-exchangers, adsorbents and an important ingredient of detergents (Breck, 1974; Baksh *et al.*, 1992; Davis, 1998; Weitkamp & Puppe, 1999; Tanabe & Hölderich, 1999; ZEODET, 2000; Pabalan & Bertetti, 2001; Kalló, 2001), zeolites and synthetic zeolite-like materials represent a fascinating class of materials covering the enormous structural variations obtainable in relative simple chemical systems (Smith, 1988; Cheetham *et al.*, 1999; Higgins, 1994; Armbruster & Gunter, 2001; Davis, 2002). Primary building units for many members of this class of materials are single TO_4 tetrahedra, where T is usually Si^{4+}, Al^{3+}, but can also be other multivalent cations. These tetrahedral units are often corner-linked to form relatively rigid units, often in the form of rings. These are further assembled to make up chain- or layer-like building units (LLBUs). Secondary building units (SBUs; Breck, 1974) are topology-specific, regular blocks of TO_4 tetrahedra derived from the assumption that the entire framework is made up of one type of SBU (Baerlocher *et al.*, 2001). In the presence of only 20 unique SBUs observed to date (Baerlocher *et al.*, 2001), the manifold variation in the structural topologies of zeolites and many zeolite-like materials can be described by different connections of SBUs. The fibrous zeolites comprise a family of structures with frameworks built with the same SBUs, 4–1 $(Si,Al)O_{10}$ tetrahedra (Fig. 1): Three

Table 1
Experimental details.

Crystal data	
Chemical formula	$H_{8.60}K_{2.60}Li_{9.40}O_{42.30}Si_{16}$
M_r	1301.80
Cell setting, space group	Monoclinic, $P2_1/m$
a, b, c (Å)	6.560 (1), 23.057 (5), 6.978 (1)
β (°)	90.08 (3)
V (Å^3)	1055.4 (4)
Z	1
D_x (Mg m^{-3})	2.048
Radiation type	Synchrotron X-ray (X3*a*1, NSLS at BNL)
No. of reflections for cell parameters	3676
θ range (°)	4.2–25.2
μ (mm^{-1})	0.65
Temperature (K)	293 (2)
Crystal form, color	Needle-like plate, colorless
Crystal size (mm)	0.1 × 0.005 × 0.001
Data collection	
Diffractometer	Bruker SMART 1K CCD
Data collection method	Rotation data aqusition using φ scans
Absorption correction	None
T_{min}	–
T_{max}	–
No. of measured, independent and observed reflections	7938, 2505, 2331
Criterion for observed reflections	$I > 2\sigma(I)$
R_{int}	0.036
θ_{max} (°)	31.3
Range of h, k, l	$-8 \Rightarrow h \Rightarrow 8$ $-30 \Rightarrow k \Rightarrow 30$ $-8 \Rightarrow l \Rightarrow 3$
Refinement	
Refinement on	F^2
$R[F^2 > 2\sigma(F^2)]$, $wR(F^2)$, S	0.092, 0.254, 0.86
No. of reflections	2505
No. of parameters	101
H-atom treatment	Constrained to parent site
Weighting scheme	$w = 1/[\sigma^2(F_o^2) + (0.1834P)^2 + 18.3702P]$, where $P = (F_o^2 + 2F_c^2)/3$
$(\Delta/\sigma)_{max}$	15.000
$\Delta\rho_{max}$, $\Delta\rho_{min}$ (e Å^{-3})	2.52, −2.15

Computer programs used: *SHELXS*97 (Sheldrick, 1990), *SHELXL*97 (Sheldrick, 1997).

different framework topologies, natrolite (NAT: Pauling, 1930; Meier, 1960), edingtonite (EDI: Taylor & Jackson, 1933; Galli, 1976; Kvick & Smith, 1983) and thomsonite (THO: Taylor *et al.*, 1933; Alberti *et al.*, 1981, Pluth *et al.*, 1985), result from varying the linkage between individual 4–1 SBUs as well as through different cross-linking of the chains of these SBUs (Armbruster & Gunter, 2001). The method of cross-linking of the same basic building blocks is directly related to the type and location of the non-framework constituents inside the channel-like voids. On the other hand, 4–1 T_5O_{10} SBUs are capable of adopting various types of framework T cations, for example, P^{5+}, Ge^{4+}, Ga^{3+}, Co^{2+} and Zn^{2+}, allowing a wide range of chemical and electrostatic changes in a given topology (Klaska & Jarchow, 1985; Xie *et al.*, 1988; Bu *et al.*, 1998; Tripathi *et al.*, 2000; Lee *et al.*, 2000; Harrison, 2001). Furthermore, the ordering and disordering of species in both the framework and the channel results in numerous structural variations in each subgroup of NAT-, EDI- and THO-type materials (Armbruster & Gunter, 2001).

The new zeolite-like lithosilicate RUB-30 (Ruhr-Universität-Bochum, phase No. 30, $K_{2.6}Li_{5.4}[Li_4Si_{16}O_{38}]\cdot 4.3H_2O$), further extends the wide chemical variance observed for 4–1 T_5O_{10} units in this class by the incorporation of mono-valent Li^+ (Park, 1998). RUB-30 exhibits none of the NAT, EDI and THO topologies due to the uncommon connection of 4–1 $LiSi_4O_{10}$ SBUs through edge-sharing $[LiO_4]$ tetrahedra. This paper presents the new topology of RUB-30 as derived from the refinement of an 'average' structure based on a subcell with a = 6.560 (1), b = 23.057 (5), c = 6.978 (1) Å, β = 90.08 (3)°. The real structure gives rise to additional superlattice reflections and diffuse streaks, as observed in an X-ray single-crystal diffraction data set collected at a higher resolution and brightness. The problem of defining *the* 'true average' structure and some hints concerning the real structure are discussed in §7.

2. Experimental

Crystals of RUB-30 were synthesized from a molar composition of $0.23LiOH:0.23KOH:0.75SiO_2:44H_2O$ with the addition of 0.08TEAOH (tetraethylammonium hydroxide) to make a more basic, clear solution. A typical synthesis of RUB-30 is as follows: 0.88 g of TEAOH (35% aqueous solution, Alfa), 0.25 g of lithium hydroxide monohydrate ($LiOH\cdot H_2O$, Alfa) and 0.39 g of potassium hydroxide (10–15% water, Aldrich) were dissolved in 20 g of distilled water. While vigorously stirring, tetramethoxysilane (2.91 ml TMOS, > 98%, Alfa) as a silicon source was slowly dropped into this solution. After aging for 1 h at room temperature, the mixture was charged into 22 ml Teflon-lined stainless steel autoclaves (Parr) and then allowed to react under autogeneous hydrothermal conditions by heating at 448–453 K for 7 d. The synthesis product was washed with distilled water several times, filtered and then dried at room temperature overnight.

The density of RUB-30 was determined with the suspension method, where diiodomethane (99%, Aldrich; ρ = 3.325 g cm^{-3}) and dimethyl formamide (J. T. Balker; ρ = 0.957 g cm^{-3}) were used as matching solutions. Chemical

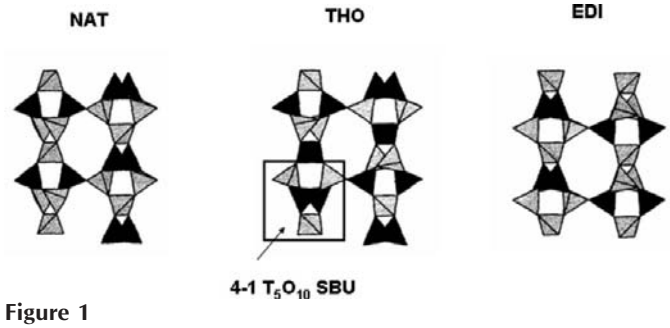

Figure 1
Variations of tetrahedral linking of 4–1 T_5O_{10} SBUs (highlighted in the square) create different chains of the units in NAT, THO and EDI framework topologies. Lighter and darker shaded tetrahedra represent $[SiO_4]$ and $[AlO_4]$ tetrahedra, respectively (Armbruster & Gunter, 2001).

analysis was performed in the chemical laboratories of the Institut für Geologie, Mineralogie und Geophysik at Ruhr Universität Bochum, Germany. The chemical components silicon and potassium of as-synthesized RUB-30 were analyzed using an electron microprobe (EMP; Cameca SX50), and lithium was determined by atomic absorption spectrophotometry (AAS; Perkin-Elmer 4000). Differential thermal analysis (DTA) and thermogravimetric analysis (TGA) measurements were carried out to observe the dehydration processes and the thermal behavior of the as-synthesized RUB-30 sample with increasing temperature in air with a heating rate of 1 K min^{-1} up to 1273 K (Setaram TG-DTA92-16.18 thermal analyzer). The crystal morphology was determined using a scanning electron microscope (Stereoscan 250, MK3D).

A single crystal ($1 \times 5 \times 100\ \mu m^3$) of as-synthesized RUB-30 was used for the structure solution with synchrotron X-ray diffraction data. The data collection was performed at the X3A beamline [wavelength = 0.643 Å; Si(111) monochromator] of the National Synchrotron Light Source (NSLS) at Brookhaven National Laboratory (BNL). Intensity data were detected on a Bruker 1K CCD (charge coupled device) area detector every 0.3° (φ) at a counting time of 10 s while rotating the crystal 0–360° (φ) at a distance of 30 mm from the detector. *SMART* software was used to collect the data and determine the orientation matrix; *SAINT* software was used for the integration of intensities, Lorentz polarization (*Lp*) correction and the final unit-cell parameter determination; no absorption correction was applied because of the low absorption due to the small crystal size ($\mu d_{max} = 0.06$). All the programs used are distributed by Bruker AXS Inc. (Bruker, 1997). Only a quarter of a total of 7938 measured reflections show intensities higher than $2\sigma(I)$, as shown in Table 1.

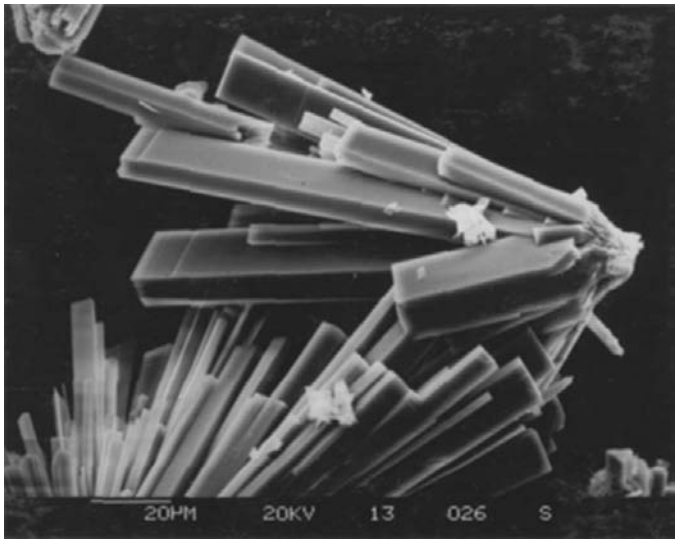

Figure 2
Scanning electron micrograph of RUB-30 crystal aggregates (as-synthesized). Besides well crystallized, thin, needle-shaped plates of RUB-30 as the main phase, fine crystals of quartz and a lithium silicate hydrate, $Li_2Si_2O_5{\cdot}2H_2O$, coexist in the bulk sample.

To detect weak reflections, another data collection was carried out using a brighter light source at beamline 13BMD of the GeoSoilEnviro Consortium for Advanced Radiation Sources (GSECARS) of the Advanced Photon Source (APS) at Argonne National Laboratory (ANL). A wavelength of 0.699 (3) Å (graphite monochromator) and a longer detector–crystal distance of 70 mm were chosen to increase the resolution. This time, a smaller crystal of RUB-30 ($\sim 0.5 \times 1 \times 100\ \mu m^3$) was mounted for the data collection to avoid extreme overexposure. Intensity data were collected on a Bruker 2K CCD area detector with a step interval of 0.3° (φ) at a counting time of 2 s per frame. A supercell ($a \times 2b \times c$) could be detected with this data set, but a strong mosaic spread of 15° made it difficult to integrate the intensities, *e.g.* resulting in strongly differing intensities of Friedel's pairs. The quality of the structure model of RUB-30 could not be improved compared with that worked out from the previous analysis using data of X3A. In the present work, we report an 'average' structure of RUB-30 determined from the analysis with X3A data. Nonetheless, the reconstruction of GSECARS raw data in reciprocal-space coordinates using *MPAUS* software, provided by Professor Reinhard B. Neder of Julius-Maximilians Universität Würzburg, Germany, allowed more ready visualization of modifications to the reciprocal lattice of the substructure, already observed in the data collected at the NSLS. The modifications included diffuse streaks along *k* and unusual superstructure reflections *hkl*, only when *k*, *l* = odd. An attempt was made to explain these new observations modifying the 'average' structure of RUB-30, as described in §7.

3. Results from the synthesis, chemical and thermal analyses

The synthesis product contained highly crystalline phases of RUB-30 as the main composite, quartz and a lithium silicate hydrate, $Li_2Si_2O_5{\cdot}2H_2O$. A typical photograph of RUB-30 crystallized in the form of needle-like thin plates is shown in Fig. 2. An average density of 2.3 (1) g cm^{-3} was determined with individual aggregates of RUB-30, which is higher than the value of 2.043 g cm^{-3} obtained from the combined chemical and structural analysis (Table 1). This discrepancy may arise from the dense phases (quartz, for example) grown in between aggregates of RUB-30. The chemical and thermal analyses resulted in $1.3K_2O{:}4.7Li_2O{:}16SiO_2{:}4.3H_2O$ for RUB-30 as synthesized. As shown in DTA/TGA (Fig. 3), a weight loss of 5–6 wt% was observed up to 473 K owing to the dehydration of RUB-30. The dehydration occurred in two steps at $\sim$ 373 and $\sim$ 473 K, which indicate the presence of differently strong-bonded water molecules in RUB-30. There are two exotherm peaks between 573 and 673 K, pointing to two phase transitions up to 673 K. After ending the DTA/TGA program at 1283 K only a mass of glass was observed, accompanying the steady weight loss up to 2–3 wt%, probably due to OH groups squeezed out with increasing temperature.

Table 2
Selected geometric parameters (Å, °).

Si1—O1	1.596 (5)	O1—Si1—O5	111.4 (3)
Si1—O5	1.610 (7)	O1—Si1—O6^{i}	109.6 (3)
Si1—O6^{i}	1.610 (6)	O5—Si1—O6^{i}	107.7 (3)
Si1—O8^{i}	1.614 (6)	O1—Si1—O8^{i}	111.7 (3)
		O5—Si1—O8^{i}	110.0 (3)
		O6^{i}—Si1—O8^{i}	106.2 (3)
Si2—O6	1.580 (6)	O2—Si2—O3^{ii}	108.0 (3)
Si2—O3^{ii}	1.603 (2)	O6—Si2—O7	111.0 (3)
Si2—O7	1.606 (6)	O3^{ii}—Si2—O7	108.9 (4)
Si2—O4	1.613 (6)	O6—Si2—O4	110.1 (3)
		O3^{ii}—Si2—O4	108.1 (4)
		O7—Si2—O4	110.7 (3)
Si3—O9^{i}	1.568 (5)	O9^{i}—Si3—O5^{iii}	114.4 (3)
Si3—O5^{iii}	1.617 (6)	O9^{i}—Si3—O7	113.5 (3)
Si3—O7	1.635 (6)	O5^{iii}—Si3—O7	107.0 (3)
Si3—O2^{iv}	1.640 (6)	O9^{i}—Si3—O2^{iv}	114.8 (3)
		O5^{iii}—Si3—O2^{iv}	104.1 (3)
		O7—Si3—O2^{iv}	101.8 (3)
Si4—O10	1.565 (5)	O10—Si4—O8^{v}	113.4 (3)
Si4—O8^{v}	1.619 (6)	O10—Si4—O4	114.3 (3)
Si4—O4	1.631 (6)	O8^{v}—Si4—O4	108.0 (3)
Si4—O2^{i}	1.631 (6)	O10—Si4—O2^{i}	114.5 (3)
		O8^{v}—Si4—O2^{i}	103.6 (3)
		O4—Si4—O2^{i}	101.9 (3)
LiF—O9^{ii}	1.937 (12)	O9^{ii}—LiF—O10^{i}	101.4 (6)
LiF—O10^{i}	1.972 (14)	O9^{ii}—LiF—O1	115.2 (6)
LiF—O1	1.993 (13)	O10^{i}—LiF—O1	115.4 (7)
LiF—O9	2.043 (14)	O9^{ii}—LiF—O9	97.4 (6)
		O10^{i}—LiF—O9	116.9 (6)
		O1—LiF—O9	109.1 (6)
K1—O*W*2^{i}	2.71 (3)	K1*B*—O4^{iv}	2.86 (1)
K1—O*W*2	2.71 (3)	K1*B*—O4^{vi}	2.86 (1)
K1—O*W*2*B*^{i}	2.88 (3)	K1*B*—O7^{i}	2.87 (1)
K1—O*W*2*B*	2.88 (3)	K1*B*—O2^{iv}	2.90 (1)
K1—O7^{i}	2.879 (8)	K1*B*—O2^{vi}	2.90 (1)
K1—O4^{iv}	2.901 (8)	K1*B*—O*W*2^{i}	2.09 (4)
K1—O4^{vi}	2.901 (8)	K1*B*—O*W*2	3.09 (4)
K1—O2^{iv}	3.069 (9)	K1*B*—O*W*2*B*^{i}	3.19 (4)
K1*C*—O2^{iv}	2.768 (7)	Li1—O*W*1	1.34 (1)
K1*C*—O2^{vi}	2.768 (7)	Li1—O*W*1*B*	1.96 (2)
K1*C*—O4^{iv}	2.91 (2)	Li1—O10^{vii}	1.95 (2)
K1*C*—O4^{vi}	2.91 (2)	Li1—O10^{iv}	2.04 (2)
K1*C*—O7^{i}	2.98 (2)	Li1—O9	2.08 (2)
Li2—O*W*2*B*	1.58 (4)	Li3—O*W*1*B*	1.61 (3)
Li2—O*W*2	1.79 (4)	Li3—O*W*2*B*^{i}	1.75 (4)
Li2—O2^{iv}	2.20 (2)	Li3—O*W*1	1.93 (3)
Li2—O7	2.31 (3)	Li3—O*W*2^{i}	2.14 (4)
Li2—O4^{vi}	2.39 (3)	Li3—O2^{viii}	2.28 (3)
		Li3—O8^{iv}	2.35 (4)
		Li3—O5	2.37 (4)
K2—O3	1.01 (1)		
K2—O4^{vii}	2.241 (9)		
K2—O4^{ii}	2.241 (9)		
K2—O7^{vii}	2.378 (10)		
K2—O7^{ii}	2.378 (10)		
K2—O6^{vii}	3.092 (9)		
K2—O6^{ii}	3.092 (9)		

Symmetry codes: (i) $x, \frac{1}{2}-y, z$; (ii) $-x, -y, -z$; (iii) $1+x, \frac{1}{2}-y, z$; (iv) $x, \frac{1}{2}-y, z-1$; (v) $1+x, y, z$; (vi) $x, y, z-1$; (vii) $-x, y-\frac{1}{2}, -z$; (viii) $x-1, y, z-1$.

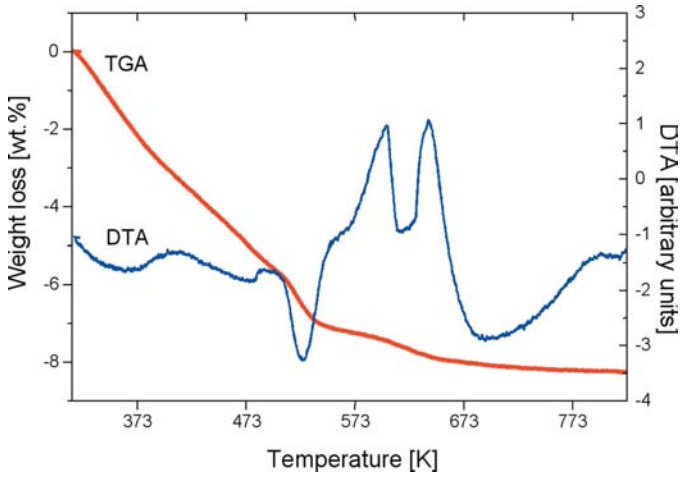

Figure 3
TGA and DTA profiles of RUB-30 showing the weight loss of *ca* 6 wt% in two steps due to the dehydration below ∼ 473 K. Condensation and breakdown of the structure occur above ∼ 533 K, which are followed by two different phase transitions between 573 and 673 K

4. Structure solution

The 'average' structure of RUB-30 has a monoclinic primitive unit cell with a = 6.560 (1), b = 23.057 (5), c = 6.978 (1) Å, β = 90.08 (3)°. The structure was solved in the space group $P2_1/m$ by direct methods, with the initial solution revealing all four Si positions (Fig. 4). Subsequent difference-Fourier syntheses located the positions of framework O atoms. Subsequent structure refinement and difference-Fourier syntheses were carried out with the program packages *SHELXTL* (Sheldrick, 1990, 1997; Bruker, 1998). For the final structure models, isotropic displacement parameters were refined along with atomic coordinates for framework Si and O atoms. Displacement parameters for extra-framework sites and for framework Li sites were fixed at reasonable values.

Difference-Fourier maps revealed three groups of split positions that were assigned to partial occupancies. The occupants of these sites were identified initially as potassium (K1/K1*B*/K1*C*) and water molecules (O*W*1/O*W*1*B*; O*W*2/O*W*2*B*), based on their coordination (Table 2 and supplementary material[1]). The entire occupancy ratio of K:H_2O = 0.25 in the unit cell obtained from the structure refinement is far from the chemical composition of RUB-30 with K:H_2O = 0.6 as obtained from the chemical analysis. Furthermore, the summation of the occupation factors for the split positions O*W*1 [= 0.92 (3)] and O*W*1*B* [= 0.70 (3)] is higher than 1. This indicates that these positions are partially occupied by additional heavier species, such as K. For this reason, the occupancy parameters at O*W*1 and O*W*1*B* were recalculated with K as being the type of occupant, resulting in 0.27 (1) and 0.21 (1) for the positions O*W*1 and O*W*1*B*, respectively (see supplementary material). In addition, the distances d(K1—O*W*2) of less than 2.8 Å are unreasonable (Table 2). These

[1] Supplementary data for this paper are available from the IUCr electronic archives (Reference: SN5028). Services for accessing these data are described at the back of the journal.

situations point to a high static disorder of K cations and water molecules, which partially occupy the spilt positions (K1/K1*B*/K1*C*), (O*W*1/O*W*1*B*) and (O*W*2/O*W*2*B*).

After having identified most of the partially occupied extra-framework sites, a difference-Fourier synthesis indicated a position in tetrahedral coordination with a distance range of ~ 2 Å to four different positions of framework O atoms, O1, O9 ($\times$ 2) and O10. The position was denoted as LiF and inserted into the model as framework Li, on the basis of known lithosilicate structures (Park, Daniels & Gies, 2000; Park, Parise, Gies, Liu, Grey & Toby, 2000; Park *et al.*, 2001, 2002, 2004). Another position found at this stage, and designated K2, lies very near to the framework, for example, d(K2—O3) $\simeq$ 1.0 Å. Without knowing its occupation, we regarded this initially as a site partially occupied by potassium. Refinement of its occupancy parameter led to an extremely large shift of electron density, $(\Delta/\sigma)_{max} = 15$ (Table 1). As will be explained in §7, the unrealistic distance of K2 to the framework in this 'average' structure is due to K2 being located in the middle of 8MRs channels, a preferred position for potassium of a superstructure variant, called type *B*.

In the final stage of the refinement, three different positions, Li1, Li2 and Li3, could be recognized as non-framework Li sites. Compared with the framework Li site (LiF), the non-framework Li sites reside at variable distances of 1.8–2.4 Å to framework O atoms and/or water molecules (Table 2). The extremely short distances between those Li cations and water molecules (Table 2) can be due to static disorder over the sites partially occupied (see supplementary material). The occupancy parameters of Li and disordered K/H_2O were calculated with group-specific isotropic displacements of 0.01 and 0.03 Å^2, respectively (see supplementary material), based on known zeolitic lithosilicate structures (Park, Daniels & Gies, 2000; Park, Parise, Gies, Liu, Grey & Toby, 2000; Park *et al.*, 2002, 2004). Owing to the high correlations between displacement and occupancy parameters of K, H_2O and non-framework Li, there are uncertainties in their calculated occupancies with regard to the chemical composition of RUB-30. Nonetheless, the combined results from the structural and chemical analysis agree with taking $(K_{2.6}Li_{5.4})^{8+}[(Li_4O_6)^{8-}$-$(Si_{16}O_{32})^0]\cdot 4.3H_2O$ to be the structure formula of RUB30, as given in Table 1.

5. Structure description of RUB-30

The framework of RUB-30 consists of one symmetry-independent [LiO_4] and four [SiO_4] tetrahedra. There are four 4–1 $LiSi_4O_{10}$ SBUs in the unit cell, where the [LiO_4] tetrahedron is strictly ordered within each single 4–1 unit (Fig. 4). Units of 4–1 $LiSi_4O_{10}$ SBUs are connected in the [010] direction alternating through corner-sharing [$O_3Si—O—SiO_3$] and edge-sharing [$O_2Li—O_2—LiO_2$] moieties, as highlighted in Fig. 4. Two O atoms involved in each edge-shared bonding are threefold coordinated with two Li atoms and one Si atom. In the unit cell, there are three such edge-sharing [$O_2Li—O_2—LiO_2$] units, making in total six framework O atoms with threefold coordination. Along the [100] and [001] directions 4–1 $LiSi_4O_{10}$ SBUs are bonded *via* corner-sharing [$O_3Si—O—SiO_3$]. The three-dimensional, 4-connected network of the corner- and edge-sharing [SiO_4] and [LiO_4] tetrahedra can be expressed by $[(Si^{IV}{}_{16}O^{II}{}_{32})(Li^{IV}{}_4\ O^{III}{}_6)]$, where superscripts denote coordination numbers.

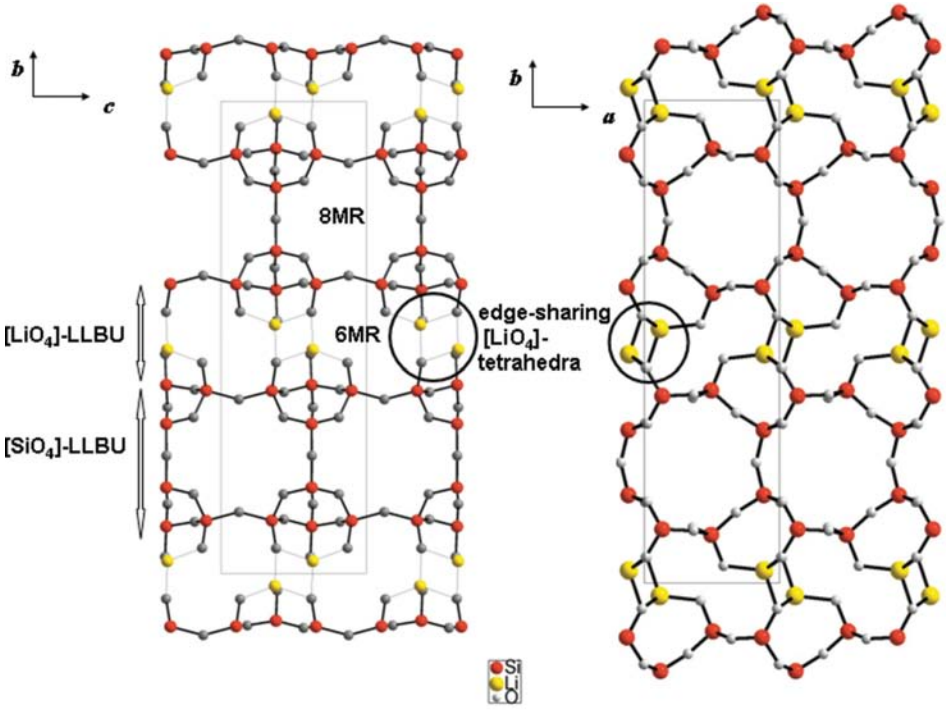

Figure 4
The framework of the 'average' structure of RUB-30 (as-synthesized): Si (large dark spheres), Li (large light spheres) and O atoms (small gray circles) build up the new open framework by alternating connections of corner-sharing [SiO_4] and edge-sharing [LiO_4] tetrahedra. The framework Li atoms are strictly ordered within each 4–1 $LiSi_4O_{10}$ SBU.

The 'average' structure of RUB-30 is an open framework and contains a three-dimensional channel system (Fig. 4): The main pore system is built with two-dimensional channels running parallel to [100] and [001], having 8MR-pore openings bounded only by corner-sharing [SiO_4] tetrahedra. The same configuration for the 8MRs channels is found in NAT, EDI and THO (Fig. 1). Parallel to the 8MRs channels, intersecting narrow 6MRs channels are attached to edge-sharing [LiO_4] tetrahedra. The third pore system of RUB-30 is confined by distorted 8MRs channels along [010].

Locations of non-framework Li and K cations along with water molecules are shown in Fig. 5: K

cations occupy the sites (K1/K1*B*/K1*C*) which are closely spaced along [100] and found in the middle of 8MRs channels on (100) (Fig. 5*a*). Chain-like water molecules are present around the middle of the distorted 8MRs channels running parallel to [010] (Fig. 5*b*). However, as mentioned in the previous section, it is more likely that potassium ions are disordered with water molecules over all those larger pore sites.

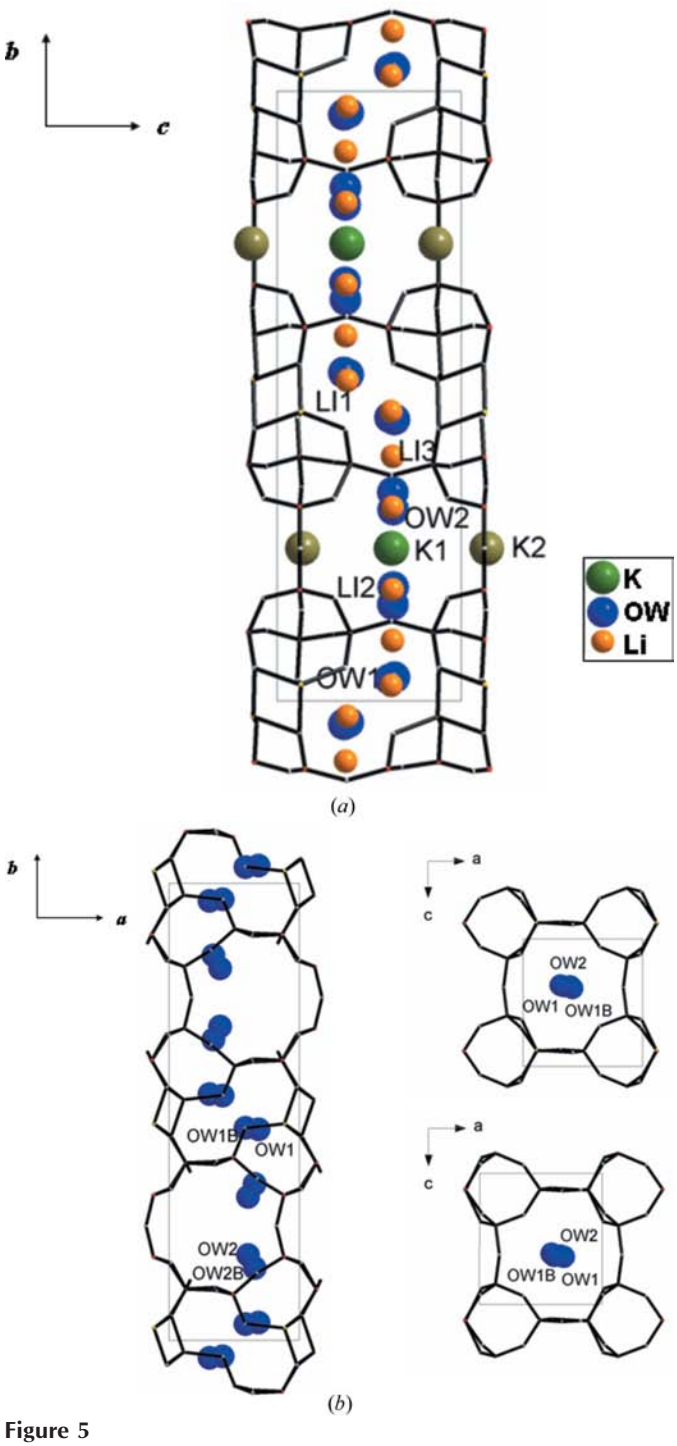

Figure 5
(*a*) Locations of extra framework K and Li cations, and water molecules in the 'average' structure of RUB-30 (as-synthesized). Strong static disorder of these pore occupancies is highly possible (see the text). The K2 site could be assigned to a suitable position for potassium and/or water molecules located in the middle of 8MRs of [SiO_4] tetrahedra in superstructure type *B* (see Fig. 7*b*), as an equivalent position to K1 in the 'average' structure. (*b*) Location of water molecules arranged in a chain-like fashion in the middle of the distorted 8MRs channel system running parallel to [010].

Non-framework Li cations are located in narrow pores close to the framework in order to compensate the negative charge of the [$LiSi_5O_{10}$] moieties: the sites Li1 and Li3 are both located within 6MR channels in the vicinity of the [LiO_4] tetrahedra, and another site, Li2, is located in the skirt of 8MR channels (Fig. 5*a*). All non-framework Li cations are threefold coordinated with framework O atoms in a distance range of 1.95 (2)–2.39 (3) Å. Unrealistically short interatomic distances, such as *d*(Li1—O*W*1) = 1.34 (1) Å, suggest statistically alternating partial occupancies, indicating that Li1 is occupied when O*W*1 is empty or *vice versa*. This statistical ordering may also be due to describing the true superstructure of RUB-30 in the substructure described here. This 'average' structure is insufficient to describe the true degree of hydration and coordination of individual non-framework Li cations. On the other hand, in the description of non-framework constituents of zeolites, this kind of 'disorder' is common (Alberti *et al.*, 1996, 1997).

6. Relation of RUB-30 to the natrolite family and other open lithosilicates

The main difference between RUB-30 and the fibrous zeolites possessing NAT, EDI or THO topologies (Fig. 1) is the presence of 6MR channels as a result of unusually bonded 4–1 SBUs by edge-sharing [LiO_4] tetrahedra. Frameworks NAT, EDI and THO display straight 8MR channels in three dimensions. Accordingly, these are more porous with lower-framework densities (FD = number of *T* atoms/1000 Å^3) than RUB-30: FD of natrolite ($Na_{16}[Al_{16}Si_{24}O_{80}]\cdot 16H_2O$) = 17.8 *T*/1000 Å (Baerlocher *et al.*, 2001); FD of RUB-30 = 18.95 *T*/1000 Å^3. However, the narrow 6MRs channel system additionally created in RUB-30 seems suited to accommodate small non-framework species such as Li cations. These differences between RUB-30 and the fibrous zeolites are due to the edge-linked nature of the Li tetrahedra and a consequence of the presence of framework Li in RUB-30.

Another feature worthy of note is the electrostatic charge of the RUB-30 framework: Only part of the total valence charge of six O atoms within four [LiO_4] tetrahedra can be compensated by the four framework Li cations, while the remaining 32 framework O atoms are charge-compensated by 16 Si atoms. The resulting total negative charge for the framework equals −8, which is balanced by the non-framework cations ($2.6K^+ + 5.4Li^+$). In other words, a charge balance of +2 per [LiO_4] framework is needed to ensure the neutrality of RUB-30. Electrostatically, the presence of edge-sharing [LiO_4] tetrahedra in the framework results in an effect equivalent to the isomorphic substitution of divalent cations such as Zn^{2+} and Be^{2+} for Si^{4+} in corner-sharing SiO_4 tetrahedra. It is well known that NAT, EDI and THO readily adopt di- and trivalent framework cations, but they do not build up

edge-sharing [TO_4] tetrahedra (Klaska & Jarchow, 1985; Xie *et al.*, 1988; Bu *et al.*, 1998; Tripathi *et al.*, 2000; Lee *et al.*, 2000; Harrison, 2001). This is probably due to strong cation–cation repulsive interactions in the edge-shared bonds. The presence of edge-sharing involving Li-centered tetrahedra in the RUB-30 framework is probably due to its low valence charge of Li^+.

RUB-30 belongs to the novel zeolite-like lithosilicates we have investigated during the past years. In terms of crystal chemistry, there are two choices, known so far, promoting the inclusion of Li^+ in open lithosilicate frameworks. The first case provides specific framework sites appropriate for Li but not for Si. In this case, a stoichiometric and high amount of Li can be introduced into the framework, being perfectly segregated from the sites for Si. In RUB-23 {$Cs_{10}(Li,H)_{14}[Li_8Si_{40}O_{96}]\cdot 12H_2O$} (Park, Daniels & Gies, 2000) and RUB-29 ($Cs_{14}Li_{24}[Li_{18}Si_{72}O_{172}]\cdot 14H_2O$) (Park, Parise, Gies, Liu, Grey & Toby, 2000; Park *et al.*, 2001), centers of each spiro-5 SBU are occupied exclusively by [LiO_4] tetrahedra. The centers of spiro-5 in RUB-23 and RUB-29 are geometrically flexible positions which are required for connecting regular LLBUs of [SiO_4] tetrahedra to build up the three-dimensional networks.

RUB-31 ($Cs_{12}Li_{13}[Li_3Zn_8Si_{37}O_{96}]\cdot 4H_2O$; Park *et al.*, 2002) and [Li–Si–O]–MFI ($TPA_4Li_8[Li_4Si_{92}O_{192}]$; Park *et al.*, 2004) represent the second case in so far as only small amounts of Li are found in well known zeolite frameworks. The low concentrations of substitution of Li for Si can be attributed to the fact that in both ANA and MFI topologies there are no distinct positions suitable for Li over Si. In these cases, the presence of small amounts of Li can cause structural distortions. Even though Li is statistically distributed on *T* sites in RUB-31 and [Li–Si–O]–MFI, the materials crystallize in lower symmetry, $P4_132$ and $P2_12_12_1$, respectively, compared with the ideal symmetry $Ia\bar{3}d$ for ANA (Taylor, 1930) and *Pnma* for MFI (van Koningsveld *et al.*, 1987). In this context, RUB-30 is the first zeolitic lithosilicate containing a high amount of framework Li atoms (Li:Si = 1: 4) which are perfectly ordered in known SBUs of zeolites.

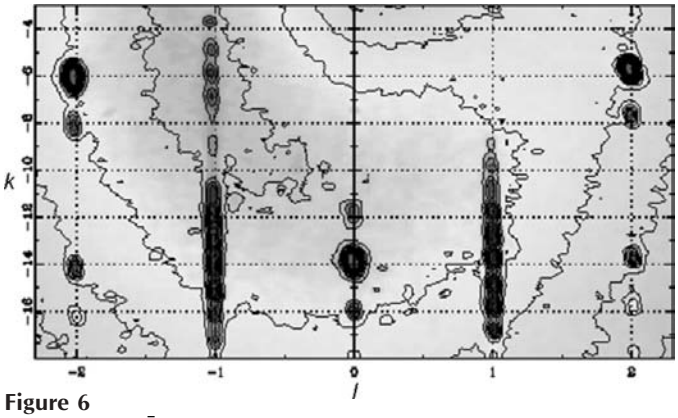

Figure 6
Reconstructed $\bar{1}kl$ plane from single-crystal diffraction data obtained at GSECARS. The indexing is based on the superstructure cell of 6.5 × 46 × 7 Å. Superstructure reflections are observed only for *l* = odd. Note that diffuse streaks also appear exclusively along the *l* = odd rows.

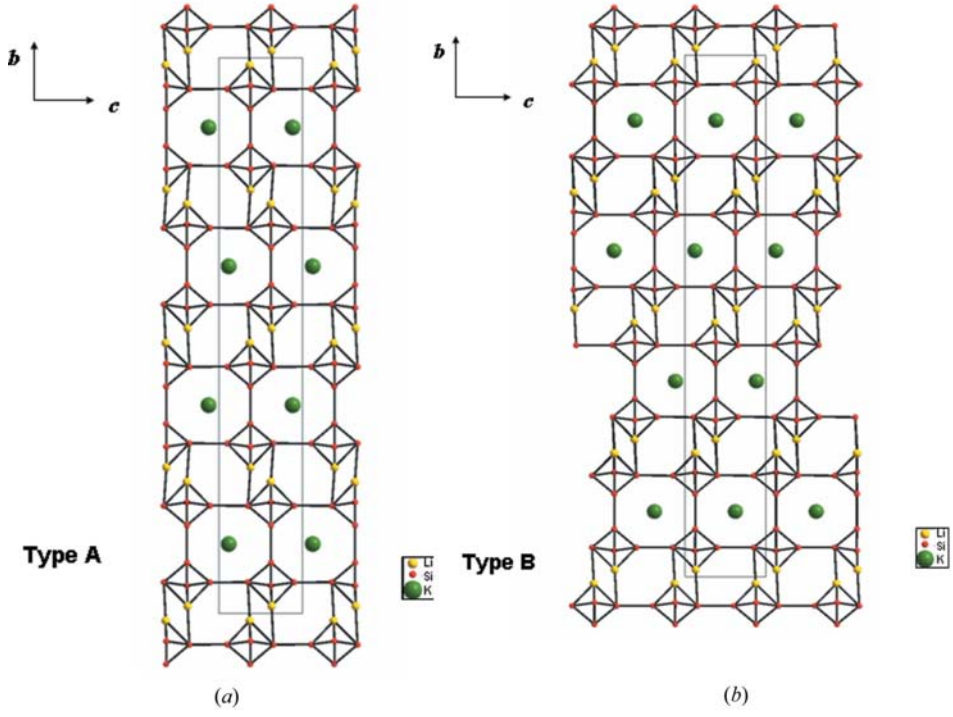

Figure 7
Framework models of types *A* and *B* for the superstructure of RUB-30. A zigzag and a diagonal arrangement of 8MR channels characterize types *A* and *B*, respectively. For clarity, only framework Si (small dark circle) and Li (middle-sized light circles) atoms are plotted along with the K atoms (large dark circle) located in 8MR channels.

7. Consideration of the superstructures of RUB-30

The superstructure of RUB-30 ($a \times 2b \times c \simeq 6.5 \times 46 \times 7$ Å^3) is characterized by unusual extinction conditions, *hkl* with *k* = odd only when *l* = odd, which is illustrated in the reconstructed layer ($\bar{1}kl$) of GSECARS data (Fig. 6). In this setting the reflections used to determine the 'average' structure of RUB-30 as presented in the previous sections obey an extinction rule *hkl* with *k* = even only, whereas the superstructure reflections obey an *A*-centering condition, *hkl* with *k* + *l* = even. There is no single symmetry group, including possible (3 + 1)-dimensional space groups if regarded as a commensu-

rate modulated structure or a composite structure (Janssen *et al.*, 1999), which can satisfy these conditions for all reflections at the same time. The presence of these diffraction features can be explained by proposing an intergrowth of two structure types *A* and *B* (Fig. 7). These types are obtained by doubling the cell constant *b* of the 'average' structure RUB-30 (see supplementary material). They comprise four LLBUs containing 6MRs channels with edge-sharing [LiO_4] tetrahedra and four other LLBUs of 8MRs channels.

Type *A* is simply the doubled 'average' structure of RUB-30 ($2 \times b$), showing a zigzag arrangement of LLBUs (Fig. 7*a*), and has the space-group symmetry $P\bar{1}$. The structure factor of type *A* ($= F_A$) can then be calculated from that of the 'average' structure ($= F_a$): $F_A = F_a[1 + \exp(2\pi ik/2)]$. The reflection intensities are $I_A = |2F_a|^2$ (observed) when k = even and $I_A = 0$ (absent) when k = odd.

Structure type *B* is constructed by shifting the subcell by $\frac{1}{2}$ along **b** and **c**. Consequently, the LLBUs are stacked differently in a diagonal rearrangement, resulting in the space-group symmetry $A\bar{1}$ (Fig. 7*b*). The structure factor of type *B* ($= F_B$) is calculated from $F_B = F_a\{1 + \exp[2\pi i(k + l)/2]\}$, leading to the required systematic extinction conditions

$I_B = |2F_a|^2$ (observed) when $k + l =$ even, and

$I_B = 0$ (absent) when $k + l =$ odd.

As a consequence, reflections *hkl* with l = odd belong alternately to type *A* for k = even and to type *B* for k = odd. On the other hand, reflections *hkl* with l = even exist for k = even only, *i.e.* their intensities contain contributions from both types *A* and *B*. As was found and can *e.g.* be seen in Fig. 6, these exactly overlapping reflections *hkl* with k, l = even have in general stronger intensities than the l = odd reflections. As a consequence, only these strong reflections could be regarded to define the 'true average' structure with lattice constants $a \times b \times c/2 \simeq 6.5 \times 23 \times 3.5$ Å^3. This 'true average' structure with an unrealistic $c/2$ repeat has been solved too. It shows all the features of the superposition of structure types *A* and *B*, but did not reveal any further insights into the real structure, and its presentation is therefore omitted here. It has to be emphasized, however, that the structure described in the preceding sections is therefore not a 'true average' structure in a strict sense as it contains the influence of type *B* only *via* the l = even reflections. This is the reason why 'average' has been put into parenthesis in the preceding paragraphs and has to be kept in mind in the following interpretation.

The unrealistic occupancy of position K2 found in the structure analysis (Fig. 5*a*) can now be explained with its location in the middle of large 8MRs pores in type *B* (Fig. 7*b*). K2 is the preferred site for K^+ in type *B*, equivalent to that of the K1 site in the middle of large 8MRs pores in type *A* (Fig. 7*a*). The low occupancy at K2 in the 'average' structure can be related to the lower frequency of the diagonal arrangement of the LLBUs of the framework.

There are diffuse streaks along *k* observed exclusively for l = odd, *i.e.* where superstructure reflections are present (Fig. 6). This can be more clearly seen on the slices of diffraction patterns cut along *k* at $l = 2$ (Fig. 8*a*) and at $l = 3$ (Fig. 8*b*). In spite of these diffuse streaks along *k* at $l = 3$, the peak widths of

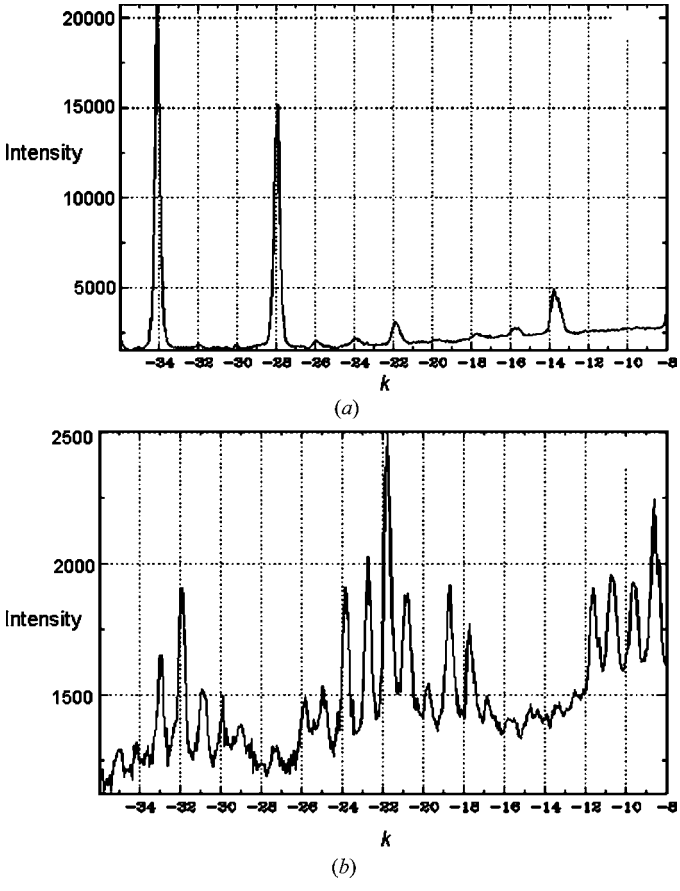

Figure 8
Diffraction pattern along (*a*) $\bar{1}k2$ and (*b*) $\bar{1}k3$ rows of the reconstructed $\bar{1}kl$ plane shown in Fig. 6: Reflections $\bar{1}k2$ (k = even) in (*a*) define the 'true average' structure. Reflections $\bar{1}k3$ (k = even) belong to structure type *A*, while $\bar{1}k3$ (k = odd) belong to type *B* in (*b*). The slice $\bar{1}k3$ shows distinct diffuse background, but $\bar{1}k2$ does not. Note that the peak width of superstructure reflections is as narrow as that of the main reflections.

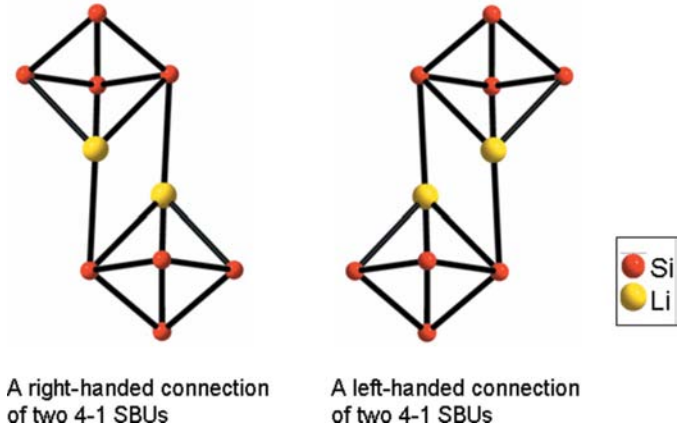

Figure 9
Two possibilities for two edge-sharing 4–1 $LiSi_4O_{10}$ tetrahedra: a right-handed and a left-handed connection. Although there is perfect ordering of framework Li atoms in individual 4–1 $LiSi_4O_{10}$ SBUs, the arrangement of these 4–1 $LiSi_4O_{10}$ SBUs can be disordered by right- and left-handed edge-sharing connections.

the superstructure reflections are as narrow as those of main reflections within the present experimental resolution. This observation indicates structure defects involving both short-range disorder and long-range order. Without disturbing the perfect ordering of Li in each 4–1 $LiSi_4O_{10}$ SBU, there are two possibilities to connect two directly neighboring 4–1 SBUs of RUB-30 *via* edge-sharing [LiO_4] tetrahedra: one connected on the right-hand side or another on the left-hand side, as shown in Fig. 9. In fact, type *A* results from perfect ordering of LLBUs *via* alternating left- and right-handed connections of edge-sharing [LiO_4] tetrahedra. Type *B* displays a perfect ordering of LLBUs *via* left-handed connections only (Fig. 7*b*). If the two alternative ways of connection were statistically random, there would be only diffuse streaking along *k* in Fig. 6, as a result of severe stacking faults of LLBUs. The real structure of RUB-30 cannot therefore involve random connections of the LLBUs. The sharpness of superstructure reflection peaks in Fig. 8(*b*) indicates that either there are large sequences of *A* and *B* resulting in intensities proportional to $\eta|F_A|^2 + (1 - \eta)|F_B|^2$ (η = fraction of type *A*), or the intergrowth is coherent resulting in $|\Sigma[F_A \exp(i\varphi i) + F_B \exp(i\varphi i)]|^2$, where the phases φ_i are determined by a suitable distribution function. In principle, these two possibilities can be distinguished by structure-factor calculations. This has been carried out for the first case and, although the limited data quality prevented a unique decision so far, the results of the structure factor calculations suggested the rejection of this possibility, *i.e.* where large slabs of *A* and *B* exist. On the other hand, the second possibility, *i.e.* a coherent intergrowth of the types *A* and *B*, requires the determination of the distribution function, which is currently under development and will be presented elsewhere. Therefore, at present, we regard the real structure of RUB-30 as a disturbed structure in which types *A* and *B* are coherently intergrown.

8. Conclusions

This paper is a full report of the synthesis of the zeolitic lithosilicate $K_{2.6}Li_{5.4}[Li_4Si_{16}O_{38}]\cdot 4.3H_2O$, its physico-chemical properties, and the complex new structure. It demonstrates that the inclusion of Li into the framework of natrolite variants impacts their structural chemistry and causes a dramatic change in their structural properties to give a new topology, RUB-30.

The observation of unusual superstructure reflections of RUB-30 and diffuse streaks could be assigned to two types of superstructures, *A* and *B*, suggesting structure defects related to locally disordered, but long-range ordered layers of 4–1 $LiSi_4O_{10}$ tetrahedra. Work still remaining would be to find the actual correlation scheme between *A* and *B* in order to show the fashion of defects in RUB-30. This can be done by analyzing the diffuse intensities in more detail, accompanied by simulation studies. Unfortunately, the current data quality was insufficient for this purpose. Synchrotron X-ray diffraction experiments with better resolution and analyzing procedures as indicated above are in progress.

SHP acknowledges financial support from Deutsche Forschungsgemeinschaft (DFG) *via* PA 1222/1-1. JBP is grateful for support from National Science Foundation (NSF, DMR-0452444). Dr Peter Eng has our special thanks for support in collecting synchrotron X-ray single-crystal data of RUB-30 at GSECARS (Sector 13) of the APS, ANL. Work performed at Sector 13 is supported by the NSF(EAR-0217473), Department of Energy (DE-FG02-94ER14466) and the State of Illinois. Use of the APS was supported by the US Department of Energy (DOE), Basic Energy Sciences, (Contract No. W-31-109-Eng-38). The NSLS at BNL is supported by the US DOE, Division of Materials Sciences and Division of Chemical Sciences (Contract No. DE-AC02-98CH10886).

References

Alberti, A., Cruciani, G., Galli, E. & Vezzalini, G. (1996). *Zeolites*, **17**, 457–461.
Alberti, A., Martucci, A., Galli, E. & Vezzalini, G. (1997). *Zeolites*, **19**, 349–352.
Alberti, A., Vezzalini, G. & Tazzoli, V. (1981). *Zeolites*, **1**, 91–97.
Armbruster, Th. & Gunter, M. E. (2001). *Reviews in Mineralogy and Geochemistry*, Vol. 45, *Natural Zeolites – Occurance, Properties, Application*, edited by D. L. Bish & D. W. Ming, pp. 1–67. Washington, DC: Mineralogical Society of America.
Baerlocher, Ch., Meier, W. M. & Olson, D. H. (2001). *Atlas of Zeolites Framework Types*, 5th ed. Amsterdam: Elsevier Science Ltd.
Baksh, M. S. A., Kikkinides, E. S. & Yang, R. T. (1992). *Sep. Sci. Tech.* **27**, 277–294.
Breck, D. W. (1974). *Zeolite Molecular Sieves. Structure Chemistry and Use.* New York: John Wiley.
Bruker (1997). *SMART* and *SAINT*. Bruker AXS Inc., Madison, Wisconsin, USA.
Bruker (1998). *SHELXTL*. Bruker AXS Inc., Madison, Wisconsin, USA.
Bu, X., Gier, T. E., Feng, P. & Stucky, G. D. (1998). *Chem. Mater.* **10**, 2546–2551.
Cheetham, A. K., Férey, G. & Loiseau, Th. (1999). *Angew. Chem. Int. Ed.* **38**, 3268–3292.
Davis, M. E. (1998). *Micropor. Mesopor. Mater.* **21**, 173–182.
Davis, M. E. (2002). *Nature*, **417**, 813–821.
Galli, E. (1976). *Acta Cryst.* B**32**, 1623–1627.
Harrison, W. T. A. (2001). *Acta Cryst.* E**57**, m248–m250.
Higgins, J. B. (1994). *Reviews in Mineralogy*, Vol. 29, *Silica-Physical Behavior, Geochemistry, and Materials Applications*, edited by P. J. Heaney, C. T. Prewitt & G. V. Gibbs, pp. 507–543. Washington, DC: Mineralogical Society of America.
Janssen, T., Janner, A., Looijenga-Vos, A. & de Wolff, P. M. (1999). *International Tables for Crystallography*, Vol. C, *Mathematical, Physical and Chemical Tables*, 2nd ed., edited by A. J. C. Wilson & E. Prince, pp. 899–947. Dordrecht: Kluwer Academic Publishers.
Kalló, D. (2001). *Reviews in Mineralogy and Geochemistry*, Vol. 45, *Natural Zeolites – Occurance, Properties, Application*, edited by D. L. Bish & D. W. Ming, pp. 519–550. Washington, DC: Mineralogical Society of America.
Klaska, K. H. & Jarchow, O. (1985). *Z. Kristallogr.* **172**, 167–174.
Koningsveld, H. van, van Bakkum, H. & Jansen, J. C. (1987). *Acta Cryst.* B**43**, 127–132.
Kvick, A. & Smith J. V. (1983). *J. Chem. Phys.* **79**, 2356–2362.
Lee, Y. J., Kim, S. J. & Parise, J. B. (2000). *Micropor. Mesopor. Mater.* **34**, 255–271.
Meier, W. E. (1960). *Z. Kristallogr.* **113**, 430–444.
Pabalan, R. T. & Bertetti, F. (2001). *Reviews in Mineralogy and Geochemistry*, Vol. 45, *Natural Zeolites – Occurance, Properties,*

Application, edited by D. L. Bish & D. W. Ming, pp. 453–518. Washington, DC: Mineralogical Society of America.
Park, S.-H. (1998). PhD Thesis, Ruhr Universität Bochum, Germany.
Park, S.-H., Daniels, P. & Gies, H. (2000). *Micorpor. Mesopor. Mater.* **37**, 129–143.
Park, S.-H., Gies, H., Toby, B. H. & Parise, J. B. (2002). *Chem. Mater.* **14**, 3187–3196.
Park, S.-H., Liu, H., Kleinsorge, M., Grey, C. P., Toby, B. H. & Parise, J. B. (2004). *Chem. Mater.* **16**, 2605–2614.
Park, S.-H., Parise, J. B. & Gies, H. (2001). *Stud. Surf. Sci. Catal.* **135**, [CD-ROM] Paper 09-O-05, edited by A. Galarneau, F. Di Renzo, F. Fajula & J. Vedrine. Amsterdam: Elsevier.
Park, S.-H., Parise, J. B., Gies, H., Liu, H., Grey, C. P. & Toby, B. H. (2000). *J. Am. Chem. Soc.* **122**, 11023–11024.
Pauling, L. (1930). *Proc. Natl Acad. Sci.* **16**, 453–459.
Pluth, J. J., Smith, J. V. & Kvick, A. (1985). *Zeolites*, **5**, 74–80.
Sheldrick, G. M. (1990). *Acta Cryst.* A**46**, 467–473.
Sheldrick, G. M. (1997). *SHELXL*97. University of Göttingen, Germany.
Smith J. V. (1988). *Chem. Rev.* **88**, 149–182.
Tanabe, K. & Hölderich, W. F. (1999). *Applied Catalysis A: General*, **181**, 399–434.
Taylor, W. H. (1930). *Z. Kristallogr.* **74**, 1–19.
Taylor, W. H. & Jackson, R. (1933). *Z. Kristallogr.* **86**, 53–64.
Taylor, W. H., Meek, C. A. & Jackson, W. W. (1933). *Z. Kristallogr.* **84**, 373–398.
Tripathi, A., Johnson, G. M., Kim, S. J. & Parise, J. B. (2000). *J. Mater. Chem.* **10**, 451–455.
Weitkamp, J. & Puppe, L. (1999). *Catalysis and Zeolites.* Berlin and Heidelberg: Springer-Verlag GmbH and Co. KG.
Xie, D., Newsam, J. M., Yang, J. & Yelong, W. B. (1988). *MRS Sym. Proc.* **111**, 147–154.
ZEODET (2000). *Zeolites for Detergents – As Nature Intended*, Association of Detergent and Zeolite Producers, CEFIC (European chemical industry council), http://www.cefic.org.